



 Cite this: *RSC Adv.*, 2021, 11, 38383

# Anisotropic response of the co-crystal of CL-20/TNT under shock loading: molecular dynamics simulation

 Yan Li, <sup>\*ab</sup> Wen-Li Yu,<sup>a</sup> Huang Huang,<sup>b</sup> Min Zhu<sup>b</sup> and Jin-Tao Wang<sup>a</sup>

Using the molecular dynamics method based on the ReaxFF force field and combining it with the multi-scale shock technique, the physical and chemical change processes of CL-20/TNT co-crystals under shock loading were studied. Shock waves with velocities of 7, 8, 9 km s<sup>-1</sup> were applied to CL-20/TNT co-crystals along the X, Y, and Z directions. The anisotropy brought by the co-crystal structure was analyzed. The results show that the temperature, stress, volume compressibility, decomposition rate, products, and the cluster of CL-20/TNT are strongly related to the direction of shock waves. With the same velocity, the shock wave along the Y direction can make the system more compressed, to obtain higher temperature and greater stress. When the velocities of shock waves are 7 km s<sup>-1</sup> and 8 km s<sup>-1</sup>, systems with a higher degree of compression have a higher degree of chemical reaction, the reactants decompose faster, and richer products are generated. When the shock wave velocity is 9 km s<sup>-1</sup>, the chemical reactions are more intense, and the differences between reactants and products due to anisotropy are small. The amounts, compositions, sizes, and mass ratios of the cluster are strongly anisotropic due to the special layered structure of the energetic co-crystal, and the evolutionary processes are closely related to the chemical reaction process. The research in this paper can provide certain support for the understanding of the shock response process of energetic co-crystals.

 Received 8th September 2021  
Accepted 30th September 2021

DOI: 10.1039/d1ra06746j

[rsc.li/rsc-advances](http://rsc.li/rsc-advances)

## 1 Introduction

The co-crystallization strategy is being pursued in pharmaceuticals and optical materials.<sup>1,2</sup> Later, the strategy has been introduced into the field of energetic materials. Co-crystallization can change the way of molecular assembly and arrangement, resolving the contradiction between energy density and safety to a certain extent, which has attracted wide attention from scholars. In 2011, Bolton and Matzger first synthesized a co-crystal material with a molecular number of 1 : 1 based on CL-20 with high energy density, high sensitivity and TNT with low energy density, low sensitivity and low cost. Its various properties are between the two elemental components, significantly reducing the sensitivity of CL-20.<sup>3</sup> Since then, scholars in the field of energetic materials have successively synthesized a variety of CL-20-based co-crystals materials.<sup>4-8</sup> Co-crystallization strategy has expanded new directions for the development of high-energy insensitive energetic materials.

To further explore the fundamental ways of co-crystallization strategy to improve material properties, scholars have carried out a lot of research work using theoretical analysis and simulations. Zhang *et al.* analyzed the energy characteristics and

safety of 41 kinds of energetic co-crystals using theoretical calculations, obtaining common factors affecting the performance of co-crystals, which provided support for the design of new materials.<sup>9-11</sup> They also analyzed the influence of crystal packing on molecular stability through quantitative calculations. The results showed that the co-crystallization can increase the interaction between molecules or improve the crystal packing mode, reducing shock sensitivity.<sup>12</sup> Based on density functional theory calculations, Liu *et al.* analyzed the behavior of the two components in CL-20/HMX co-crystals under high pressure.<sup>13</sup> Xue *et al.* used the molecular dynamics method based on the ReaxFF force field to compare the thermal decomposition processes between the CL-20/HMX co-crystals and single crystals of two components. The study believed that co-crystallization was achieved by changing the internal stability and intermolecular interaction to improve overall stability.<sup>14</sup> Liu conducted a simulation study on the thermal decomposition process of the CL-20/TNT co-crystals, and later he also explored the process of reaction flow propagation in the CL-20/TNT co-crystals.<sup>15,16</sup> Guo compared the thermal decomposition processes of the CL-20/TNT co-crystals, single crystals of the two components and a simple physical mixing system. The results showed that co-crystallization can well reconcile the two components. At the same time, the energy release of the co-crystals in the early stage of the reaction is slower than that of the physical mixing system.<sup>17</sup> By analyzing the thermal

<sup>a</sup>*Xi'an High-Tech Research Institute, Xi'an 710025, China*
<sup>b</sup>*Naval University of Engineering, Wuhan 430033, China*


decomposition processes of two typical co-crystals of CL-20/TNT and CL-20/HMX, Ren summarized the three stages of thermal decomposition of CL-20-based co-crystals.<sup>18</sup>

In the actual production, storage, transportation and use of energetic materials, in addition to the thermal action from the outside, they are also likely to be shocked. A lot of theoretical research has been carried out on this aspect. He *et al.* used the SCC-DFTB (self-consistent charge density functional tight binding) method to study the initial decomposition mechanism of HMX and TATB under shock.<sup>19,20</sup> Liu's research on the reaction process of TNT under shock shows that the formation of TNT dimer has a great influence on shock sensitivity.<sup>21</sup> Huang studied the anisotropy of shock sensitivity of insensitive explosive TATB, finding that the unique intermolecular hydrogen bond and different compressibility are the main reasons for the anisotropy of shock sensitivity.<sup>22</sup> Xue used molecular dynamics to study the effect of dislocations on the shock sensitivity of RDX.<sup>23</sup> Later, a similar method was used to study the initial decomposition mechanism of CL-20 under the action of shock waves with velocities of 8–11 km s<sup>-1</sup>. The results show that the shock wave velocity has a great influence on the reaction path, products and cluster formation.<sup>24</sup> Liu studied the initial decomposition mechanism of CL-20/HMX co-crystals under a steady shock wave.<sup>25</sup> Zhang used quantitative calculations to study the initial decomposition process of CL-20/TNT co-crystals under shock.<sup>26</sup> The above researches are mainly based on the balance impact process simulation method of multi-scale shock technology. Other studies have simulated the response process of energetic materials such as TATB, PETN, RDX, HMX and ICM-102 by the non-equilibrium impact method.<sup>27–31</sup>

A large number of theoretical studies on energetic co-crystals mainly focus on the analysis of its thermal decomposition process, the comparative understanding of the thermal decomposition process of co-crystals and single crystals of their components is relatively sufficient. People also have a deep understanding of the shock response of energetic single crystals. Nevertheless, there are relatively few studies on the response process of energetic co-crystals under shock, especially the anisotropy of shock response caused by the layered structures of co-crystals that have not been reported. In this work, the anisotropy of the response of the typical energetic co-crystals CL-20/TNT under shock is studied theoretically, to provide a reference for the understanding of the shock sensitivity of energetic co-crystals and the design of new energetic co-crystals materials.

## 2 Methods and computational details

Co-crystals cell data on CL-20/TNT used in this work were derived from the X-ray crystal structure.<sup>3</sup> The initial single-crystal cell contains 8 CL-20 molecules and 8 TNT molecules. Based on this, the single-crystal cell was expanded to a 4 × 2 × 1 supercell, which contains 64 CL-20 molecules and 64 TNT molecules, totaling 3648 atoms.

Firstly, the conjugate gradient algorithm was used to relax the co-crystal structures. The convergence tolerance of force was

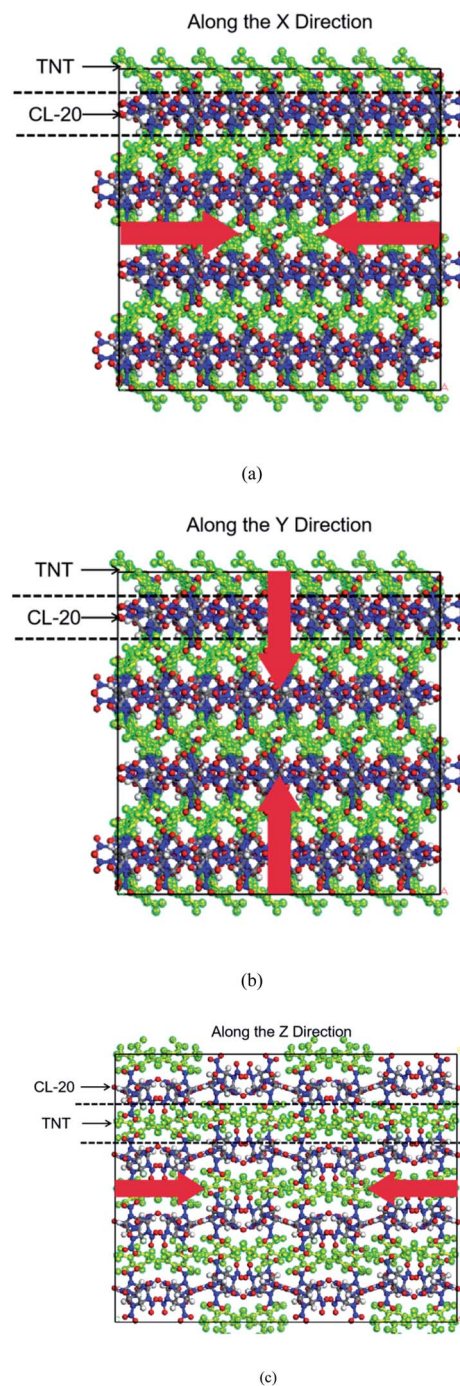


Fig. 1 Schematic diagram of shock wave action.

$10^{-7}$  kcal mol<sup>-1</sup> Å<sup>-1</sup>. Subsequently, we carried out a canonical ensemble (NVT) MD simulation each for 10 ps at 298 K using the Berendsen thermostat to relax the supercell. To obtain the structure at atmospheric pressure, the NPT ensemble was used for 15 ps relaxation at 298 K and 0 GPa, the Nosé–Hoover method was selected for temperature and pressure controls. The co-crystals structure of CL-20/TNT at room temperature and pressure was obtained, the density was 1.89 g cm<sup>-3</sup>. Then, steady shock waves with velocities of 7, 8 and 9 km s<sup>-1</sup> were loaded along X, Y and Z using multi-scale shock technology.

There were 9 simulations with 0.1 fs timestep, periodic boundary conditions and total durations of 50 ps. All simulations use the Lammmps package, the potential function was ReaxFF/lg.<sup>32</sup> The action directions of shock waves are shown in Fig. 1.

### 3 Results and discussion

#### 3.1 Evolution of temperature, stress and volume

The temperature evolution of the co-crystal system under shock-wave loading along different directions with different velocities is shown in Fig. 2. The temperature rose under various conditions. Under the shock wave with a velocity of  $7 \text{ km s}^{-1}$ , the temperature rose sharply in the initial stage and then remained stable. Under the shock wave with a velocity of  $8 \text{ km s}^{-1}$ , the temperature rose sharply in the initial stage and then rose at a slower rate. Under the shock wave with a velocity of  $9 \text{ km s}^{-1}$ , the rise of the temperature underwent 3 stages: rose sharply, rose rapidly and rose slowly. In the initial stage, the shock wave led to a physical change in the system, resulting in a sharp temperature rise. At  $7 \text{ km s}^{-1}$ , the rising temperature could not lead to a certain scale chemical reaction, making the temperature remain stable. At  $8 \text{ km s}^{-1}$ , the rising temperature could lead to a certain scale chemical reaction, making the temperature rise at a slower rate. At  $9 \text{ km s}^{-1}$ , the rising temperature could lead to a large-scale chemical reaction, making the temperature rise rapidly. After that, the chemical reaction rate slowed down and the system temperature rose at a slow rate. Comparing changes of the system temperature caused by the shock wave with the same velocity in different directions, it can be found that the shock wave loaded along the Y direction makes the temperature of the system higher than that along the X direction and Z direction. It shows that the shock temperature response of CL-20/TNT co-crystals has a certain anisotropy, which is caused by its special layered structure.

The stress evolution of the co-crystal system under shock-wave loading along different directions with different velocities is shown in Fig. 3. Under all conditions, the shock wave will lead to the rise of system stress. The overall trends are to rise rapidly at the beginning and fluctuate within a certain range when reaching a certain value. Comparing the changes of

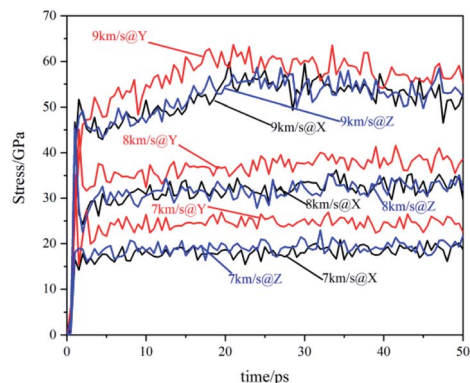


Fig. 3 Evolution of stress.

system stress caused by shock waves along the same direction with different velocities, it can be seen that the shock wave with higher velocity led to higher stress. Comparing the changes in the system stress caused by shock wave loading along with different directions with the same velocity, it was found that the shock wave loaded along the Y direction made the system stress significantly higher than that along the X direction and Z direction. This shows that the shock stress response of CL-20/TNT has a certain anisotropy, which is also related to its special layered structure.

The volume evolution of the co-crystal system under shock-wave loading along different directions with different velocities is shown in Fig. 4. The value given in the figure is the ratio of the current volume to the volume before the shock wave, which reflects the degree of compression. It can be observed from the figure that the shock wave will cause the system to be compressed under all conditions. Along the same direction, the shock wave with higher velocity led to a higher degree of compression. With the same velocity, the volume change curves caused by shock waves along different directions are similar, but the compression degree along the Y direction is significantly higher than that along X and Z directions, that is, the Y direction is easier to be compressed.

Zhang's research found that the higher degree of compression would lead to the higher temperature and stress of the CL-

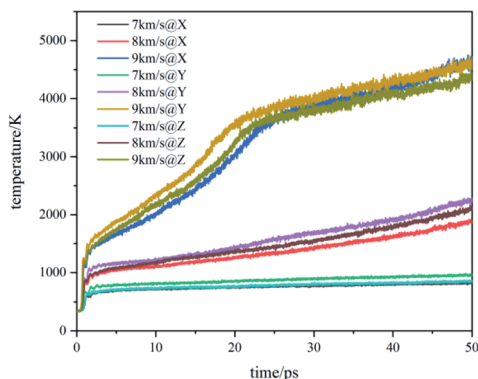


Fig. 2 Evolution of temperature.

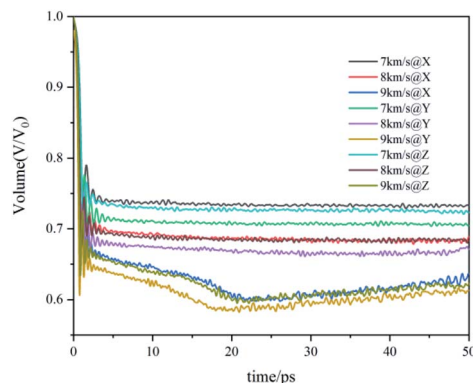


Fig. 4 Evolution of volume.



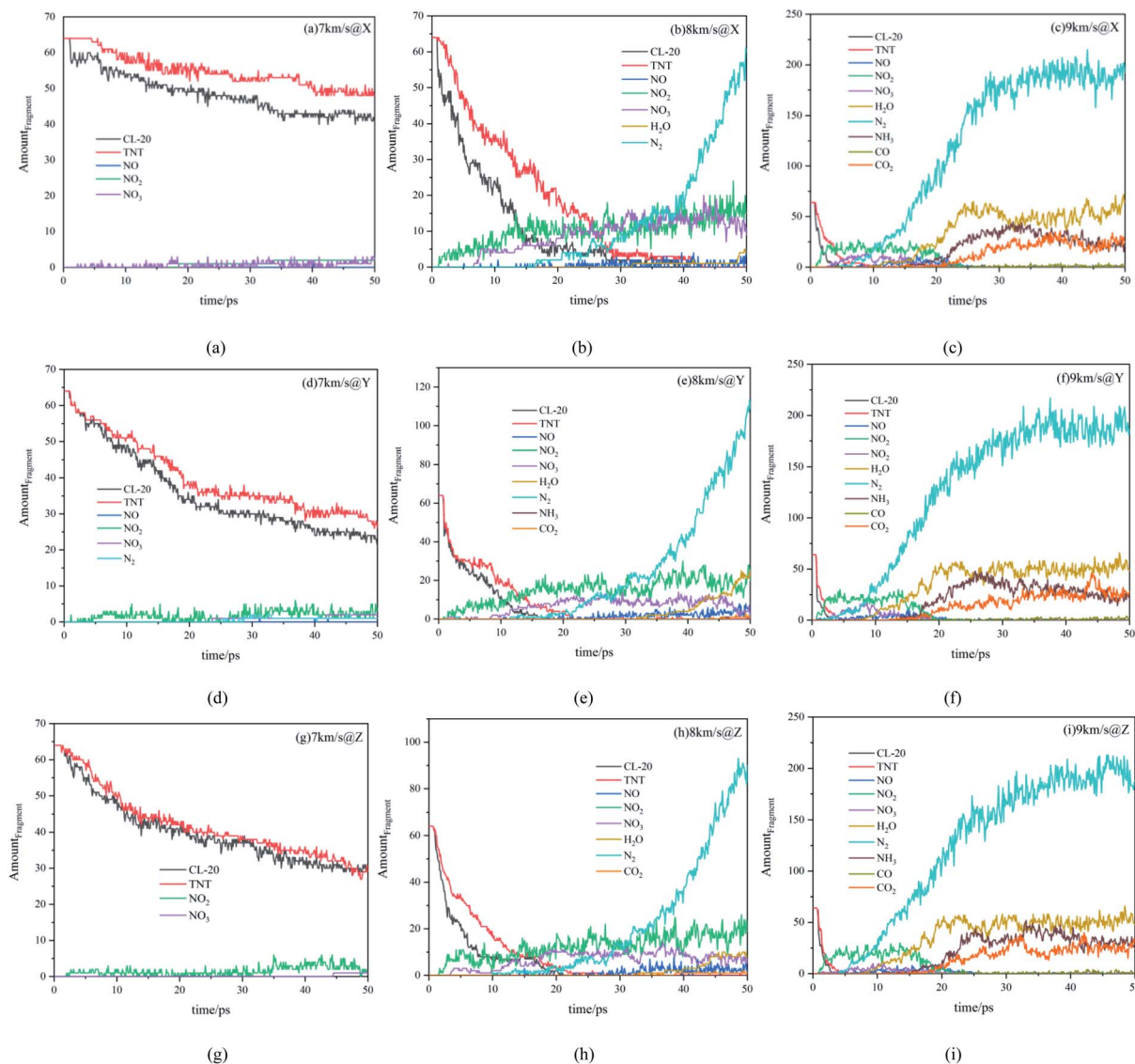


Fig. 5 Evolution of reactants and products.

20/TNT system.<sup>18</sup> According to the above analysis of temperature, stress and volume evolution information, it is found that there are obvious differences between the shock wave loaded along the Y direction and X, Z directions. The Y direction is easier to be compressed, resulting in higher temperature and stress in the system, which will lead to obvious differences in the process of the reaction.

### 3.2 Reactants and products

Fig. 5 shows the amount evolution curves of reactants and products under various conditions. Firstly, we analyze the decomposition of reactants CL-20 and TNT. When the shock wave with higher velocity was loaded, the reactants decomposed more rapidly and completely. Under the shock wave with a velocity of  $7 \text{ km s}^{-1}$ , the reaction degree of the whole system was very low, CL-20 and TNT did not decompose completely within 50 ps. Under the shock wave with a velocity of  $8 \text{ km s}^{-1}$ ,

the decomposition rate of reactants was accelerated, reactants decomposed completely within 50 ps. Under the shock wave with a velocity of  $9 \text{ km s}^{-1}$ , the reactants almost decomposed

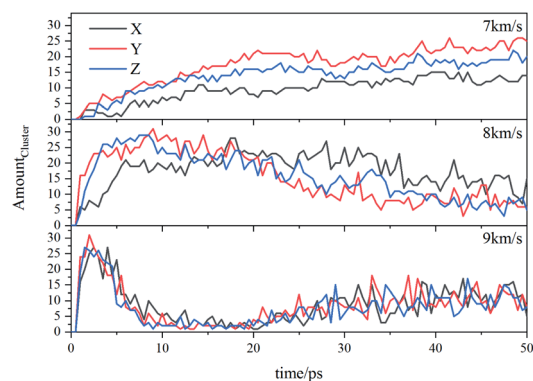


Fig. 6 Evolution of cluster amount.

completely in 10 ps. Comparing the effects of shock waves with the same velocity along with different directions, it can be observed that the decomposition rate of the system along the *Y* direction is the fastest, that along the *Z* direction is the second, and that along the *X* direction is the lowest.

Then, we analyze the main intermediates. Under the shock wave with a velocity of  $7 \text{ km s}^{-1}$ , the reaction degree of the system was low, there was only a small amount of  $\text{NO}$ ,  $\text{NO}_2$  and  $\text{NO}_3$  within 50 ps. Under the shock wave with a velocity of  $8 \text{ km s}^{-1}$ , within 50 ps, there were certain amounts of  $\text{NO}$ ,  $\text{NO}_2$  and  $\text{NO}_3$  in the system, indicating that the whole reaction continued at a certain rate. Under the shock wave with a velocity of  $9 \text{ km s}^{-1}$ , the intermediate products  $\text{NO}$ ,  $\text{NO}_2$  and  $\text{NO}_3$  were rapidly produced at the beginning and almost consumed within 20 ps, indicating that the reaction developed rapidly at the beginning, completed the large-scale reaction process in a short time, and then slowed down.

Finally, we analyze the final products. With the velocity of  $7 \text{ km s}^{-1}$ , there was no final product along the *X* and *Z* directions. However, along the *Y* direction, due to the higher degree of compression, the temperature and stress were also higher, the reaction degree was improved, a small amount of  $\text{N}_2$  was produced. With a velocity of  $8 \text{ km s}^{-1}$ , along the *X* direction there was a certain amount of  $\text{N}_2$  (63 at 50 ps), and a small amount of  $\text{H}_2\text{O}$ . Along the *Z* direction, there was more  $\text{N}_2$  (90 at 50 ps) and  $\text{H}_2\text{O}$ , there was even a small amount of  $\text{CO}_2$  in the system, indicating that the carbon rings in the system had begun to break and form small molecules containing carbon. Along the *Y* direction, there was the largest amount of  $\text{N}_2$  (115 at 50 ps) and  $\text{H}_2\text{O}$ , there was also a small amount of  $\text{CO}_2$  in the system. At the same time, there was a small amount of  $\text{NH}_3$ . With a velocity of  $9 \text{ km s}^{-1}$ , large-scale chemical reactions took place in the system in a short time. The final products were mainly  $\text{N}_2$ ,  $\text{H}_2\text{O}$ ,  $\text{CO}$ ,  $\text{CO}_2$  and  $\text{NH}_3$ , which were significantly more than those at  $8 \text{ km s}^{-1}$ . The differences between different directions were relatively small.

From the evolution of reactants and products of the system, it can be seen that the velocity of the shock wave can directly affect the decomposition of reactants, the types and number of products. The shock wave with higher velocity, made reactants decompose more rapidly and completely, leading to richer products. In addition, under the shock wave with the same velocity along different directions, the changes in reactants and products showed anisotropy. The shock wave along the *Y* direction can bring greater compression, greater stress and higher temperature, resulting in faster decomposition of reactants and richer stable products.

### 3.3 Cluster

**3.3.1 Amount of cluster.** The evolution of cluster amount is shown in Fig. 6. Under the shock wave with a velocity of  $7 \text{ km s}^{-1}$ , the amount of cluster continued to rise. The amount along the *Y* direction was the most; that along the *Z* direction was the second. The shock caused the system to be compressed, the distance between atoms decreased, the probability of mutual collision increased, and clusters continued to be generated.

Under the shock wave with a velocity of  $8 \text{ km s}^{-1}$ , the amount of cluster rose rapidly at the beginning and gradually decreased after reaching the peak. The shock caused the system to be compressed rapidly, more clusters are produced in a shorter time. After that, chemical reactions occurred, part of the cluster gradually decomposed into smaller molecules. In the first increasing stage, shock waves along the *Y* direction induced greater compression of the system, there were more clusters generated. Nevertheless, in the next decreasing stage, shock waves along the *Y* direction induced more intense chemical reactions, there was more cluster decomposition. Under the shock wave with a velocity of  $9 \text{ km s}^{-1}$ , the number of clusters

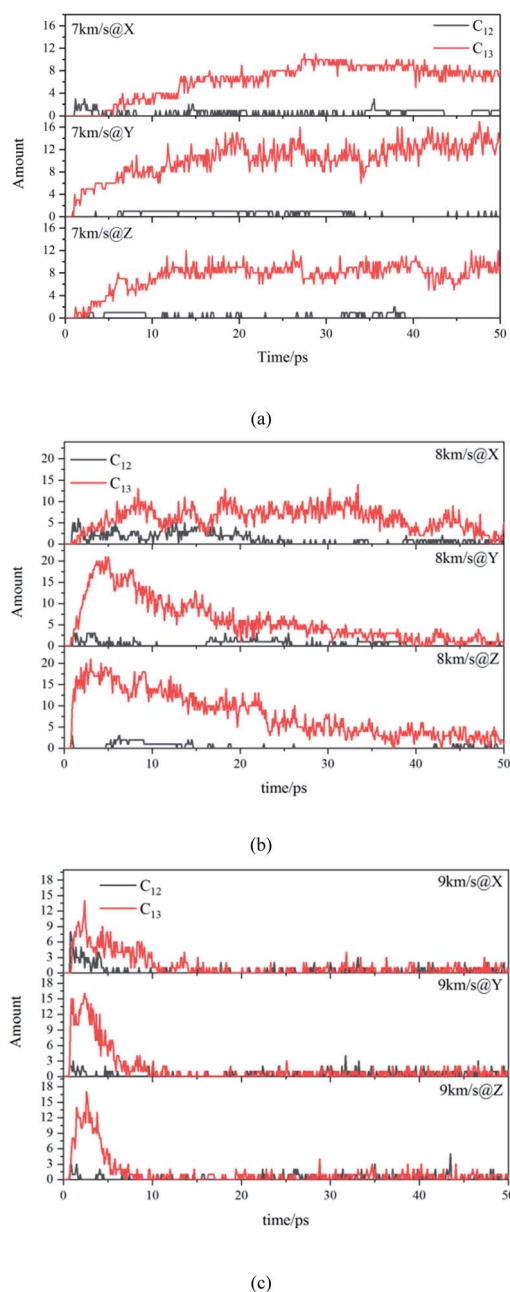


Fig. 7 Evolution of  $C_{12}$  and  $C_{13}$ .

rose sharply at the beginning, then decreased rapidly, finally fluctuating within a certain range. As previously analyzed, there were three stages of evolution: high compression stage, large-scale chemical reaction stage and stabilization stage. Due to the high intensity of shock waves, there were few differences in the action direction of shock waves.

**3.3.2 Composition of cluster.** Through analysis of the data, it can be noted that certain amounts of  $C_{12}$  and  $C_{13}$  appear in the cluster. CL-20 contains 6 carbon atoms in one molecule and TNT contain 7 carbon atoms in one molecule. That is,  $C_{12}$  is a cluster composed of two CL-20 molecules, and  $C_{13}$  is a cluster composed of one CL-20 molecule and one TNT molecule. Fig. 6 shows the changes in the amounts of  $C_{12}$  and  $C_{13}$  in the system. At  $7 \text{ km s}^{-1}$ , along the  $X$  direction,  $C_{12}$  was generated at 1 ps, the total amount of  $C_{12}$  was the most with this velocity,  $C_{13}$  was generated at 4 ps. Along the  $Y$  direction,  $C_{13}$  was generated at 1 ps, the total amount of  $C_{13}$  was the largest with this velocity,  $C_{12}$  only existed in a small amount in the subsequent part of the time. Along the  $Z$  direction,  $C_{13}$  was generated at 1 ps,  $C_{12}$  also existed only in a small amount in the subsequent part of the time. At  $8 \text{ km s}^{-1}$ , along the  $X$  direction, there was a considerable amount of  $C_{12}$  in the system, and the peak amount of  $C_{13}$  was the lowest with this velocity. Along the  $Y$  and  $Z$  direction, a large amount of  $C_{13}$  was generated in the initial stage, their amounts gradually decreased after reaching the peak, there was a certain amount of  $C_{12}$ . At  $9 \text{ km s}^{-1}$ , due to the violent chemical reaction in the system, the differences mainly existed before 10 ps. The sum of  $C_{12}$  and  $C_{13}$  along each direction had little difference. Along the  $X$  direction, the amount of  $C_{12}$  was more, and the corresponding amount of  $C_{13}$  was less. From the composition of the cluster under different shock waves, we can find that along the  $X$  direction, the probability of forming CL-20 dimers in the system is higher than that along other directions, and the probability of one CL-20 molecule binding to one TNT is relatively low. As shown in Fig. 1, due to the special layered structure of the co-crystals system, there will be great differences in the aggregation mode between molecules under shock waves along different directions, resulting in the anisotropy of the system responses.

**3.3.3 Size distribution and mass ratio of cluster.** Fig. 7 shows the distribution of cluster sizes in the system under different conditions. At  $7 \text{ km s}^{-1}$ , along the  $X$  direction, the total amount of cluster was the least, most of the cluster was concentrated in  $C_{13}$ – $C_{22}$ . Along the  $Y$  direction, the total amount of cluster was the most and most of the cluster was concentrated in  $C_{13}$ – $C_{22}$ . Along the  $Z$  direction, the total amount of cluster was in the middle, most of the cluster was concentrated in  $C_{13}$ – $C_{22}$ , but there was still a certain number of larger  $Z$  clusters. At  $8 \text{ km s}^{-1}$ , the sizes of clusters along the  $X$  direction were small in the early stage, and the distribution along the  $Y$  direction was similar to that along the  $Z$  direction. At  $9 \text{ km s}^{-1}$ , the shock wave intensity was high, and the differences caused by different directions were relatively small.

Due to the large differences in the sizes of clusters, the amount cannot comprehensively describe the overall situation of the cluster in the system. It is also necessary to analyze the mass ratios of the cluster. The mass ratio of the cluster is the

ratio of the total mass of the cluster to the total mass of all atoms in the system. As shown in Fig. 8, at  $7 \text{ km s}^{-1}$ , along the  $X$  direction the mass ratio of the cluster was the smallest. There is

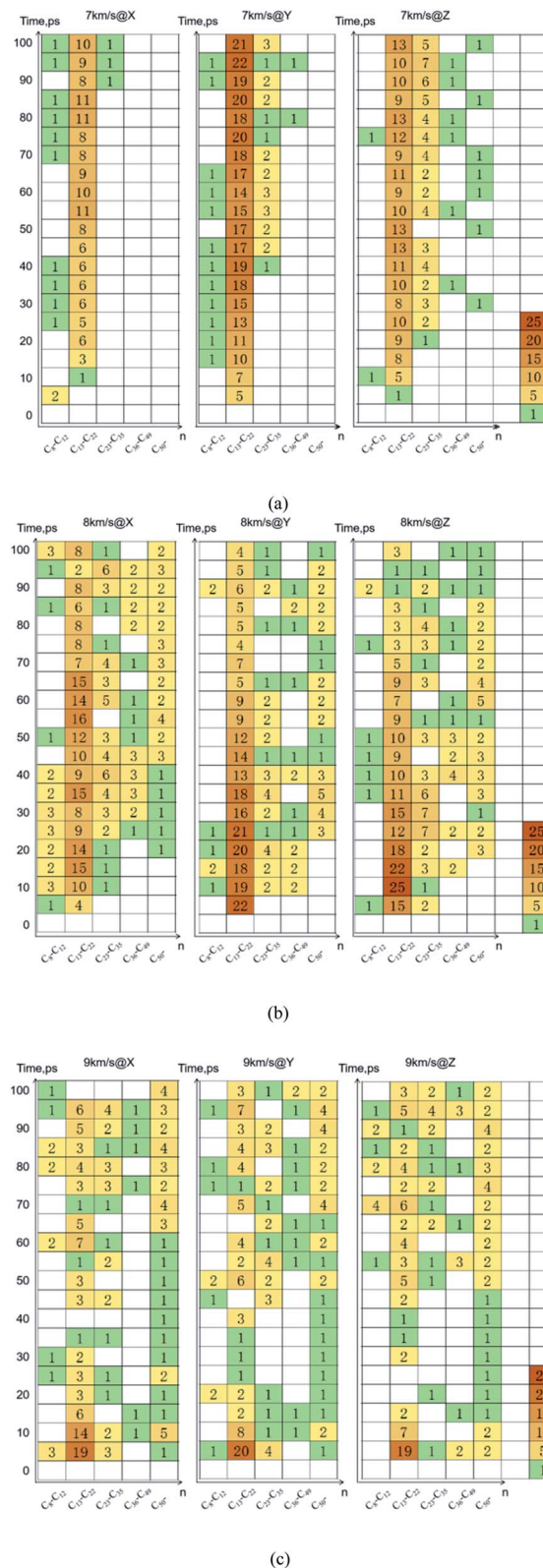


Fig. 8 Cluster size distribution.



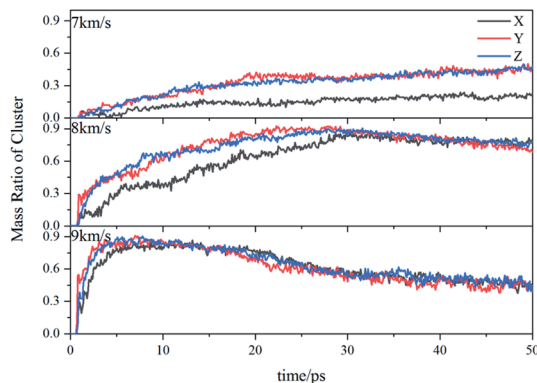


Fig. 9 Mass ratio of cluster evolution.

a certain gap in the amounts of the cluster along the *Y* direction and the *Z* direction, but the differences in cluster sizes lead to similar mass ratios of the two. At  $8 \text{ km s}^{-1}$ , due to the small size of the cluster along the *X* direction in the early stage, the mass ratio was relatively low. In the second half, the mass ratios in each direction were relatively close. At  $9 \text{ km s}^{-1}$ , as previously analyzed, the shock wave intensity was high enough, and the differences caused by different directions were relatively small (Fig. 9).

## 4 Conclusions

ReaxFF force field and multi-scale impact technology were used for generating shock waves with velocities of 7, 8,  $9 \text{ km s}^{-1}$  that were loaded into CL-20/TNT co-crystals along with *X*, *Y* and *Z* directions, respectively. The response processes of energetic co-crystals under shock waves were simulated, and the anisotropy in the response process was analyzed. The results show that:

(1) With the same velocity, compared with the shock wave along the *X* direction and *Z* direction, the shock wave along the *Y* direction will make the compression degree of the system higher, resulting in higher temperature, higher stress and a higher degree of chemical reactions.

(2) From the evolution of reactants and reaction products, along the *Y* direction the reactants decompose more rapidly and the types of products are more abundant.

(3) In terms of cluster evolution, due to the special structure of CL-20/TNT co-crystals, when the shock waves are weak, the amounts, compositions, sizes and mass ratios of clusters show obvious anisotropy. When the shock waves are strong enough, this anisotropy is not obvious.

## Conflicts of interest

There are no conflicts to declare.

## Notes and references

1 S. Cherukuvada, R. Kaur and T. N. G. Row, Co-crystallization and small molecule crystal form diversity: from

- pharmaceutical to materials applications, *CrystEngComm*, 2016, **18**, 8528.
- 2 S. A. Ross, D. A. Lamprou and D. Douroumis, Engineering and manufacturing of pharmaceutical co-crystals: a review on solvent-free manufacturing technologies, *Chem. Commun.*, 2016, **52**, 8772.
- 3 O. Bolton and A. J. Matzger, Improved Stability and Smart-Material Functionality Realized in an Energetic Cocrystal, *Angew. Chem., Int. Ed.*, 2011, **50**, 8960.
- 4 O. Bolton, L. R. Simke, P. F. Pagoria and A. J. Matzger, High Power Explosive with Good Sensitivity: A 2:1 Cocrystal of CL-20:HMX, *Cryst. Growth Des.*, 2012, **12**, 4311.
- 5 Y. Wang, Z. Yang, H. Li, X. Zhou, Q. Zhang, J. Wang and Y. Liu, A Novel Cocrystal Explosive of HNIW with Good Comprehensive Properties, *Propellants, Explos., Pyrotech.*, 2014, **39**, 590.
- 6 H. Xu, X. Duan, H. Li and C. Pei, A novel high-energetic and good-sensitive cocrystal composed of CL-20 and TATB by a rapid solvent/non-solvent method, *RSC Adv.*, 2015, **5**, 95764.
- 7 B. Duan, Y. Shu, N. Liu, B. Wang, X. Lu and Y. Lu, Direct insight into the formation driving force, sensitivity and detonation performance of the observed CL-20-based energetic cocrystals, *CrystEngComm*, 2018, **20**, 5790.
- 8 C. Huang, J. Xu, X. Tian, J. Liu, L. Pan, Z. Yang and F. Nie, High-Yielding and Continuous Fabrication of Nanosized CL-20-Based Energetic Cocrystals via Electro spraying Deposition, *Cryst. Growth Des.*, 2018, **18**, 2121.
- 9 C. Zhang, Y. Cao, H. Li, Y. Zhou, J. Zhou, T. Gao, H. Zhang, Z. Yang and G. Jiang, Toward low-sensitive and high-energetic cocrystal I: evaluation of the power and the safety of observed energetic cocrystals, *CrystEngComm*, 2013, **15**, 4003.
- 10 C. Zhang, X. Xue, Y. Cao, J. Zhou, A. Zhang, H. Li, Y. Zhou, R. Xu and T. Gao, Toward low-sensitive and high-energetic co-crystal II: structural, electronic and energetic features of CL-20 polymorphs and the observed CL-20-based energetic-energetic co-crystals, *CrystEngComm*, 2014, **16**, 5905.
- 11 X. Wei, A. Zhang, Y. Ma, X. Xue, J. Zhou, Y. Zhu and C. Zhang, Toward low-sensitive and high-energetic cocrystal III: thermodynamics of energetic-energetic cocrystal formation, *CrystEngComm*, 2015, **17**, 9037.
- 12 Q. Zeng, Y. Ma, J. Li and C. Zhang, Energy decomposition of intermolecular interactions in energetic co-crystals, *CrystEngComm*, 2017, **19**, 2687.
- 13 Z. Liu, Q. Wu, W. Zhu and H. Xiao, Insights into the roles of two constituents CL-20 and HMX in the CL-20:HMX cocrystal at high pressure: a DFT-D study, *RSC Adv.*, 2015, **5**, 34216.
- 14 X. Xue, Y. Ma, Q. Zeng and C. Zhang, Initial Decay Mechanism of the Heated CL-20/HMX Cocrystal: A Case of the Cocrystal Mediating the Thermal Stability of the Two Pure Components, *J. Phys. Chem. C*, 2017, **121**, 4899.
- 15 H. Liu, Z. Yang and Y. He, Atomistic Simulation on Pyrolysis Mechanism of CL-20/TNT Cocrystal Explosive, *Chin. J. Explos. Propellants*, 2017, **40**, 14.

- 16 H. Liu, Z. Yang and Y. He, Reactive Flow Propagation in CL-20/TNT Co-crystal Explosive Induced by Local High Temperature Zones: ReaxFF Molecular Dynamics Simulations, *Chin. J. Energ. Mater.*, 2017, **25**, 557.
- 17 D. Guo, Q. An, S. Zybin, W. Goddard, F. Huang and B. Tang, The co-crystal of TNT/CL-20 leads to decreased sensitivity toward thermal decomposition from first principles based reactive molecular dynamics, *J. Mater. Chem. A*, 2015, **3**, 5409.
- 18 C. Ren, H. Liu, X. Li and L. Guo, Decomposition mechanism scenarios of CL-20 co-crystals revealed by ReaxFF molecular dynamics: similarities and differences, *Phys. Chem. Chem. Phys.*, 2020, **22**, 2827.
- 19 Z. H. He, J. Chen, G. F. Ji, L. M. Liu, W. J. Zhu and Q. J. Wu, Dynamic Responses and Initial Decomposition under Shock Loading: A DFTB Calculation Combined with MSST Method for  $\beta$ -HMX with Molecular Vacancy, *J. Phys. Chem. B*, 2015, **119**, 10673.
- 20 Z. H. He, J. Chen and Q. Wu, Initial Decomposition of Condensed-Phase 1,3,5-Triamino-2,4,6-trinitrobenzene under Shock Loading, *J. Phys. Chem. C*, 2017, **121**, 8227.
- 21 H. Liu, Y. He, J. Li, Z. Zhou, Z. Ma, S. Liu and X. Dong, ReaxFF molecular dynamics simulations of shock induced reaction initiation in TNT, *AIP Adv.*, 2019, **9**, 015202.
- 22 X. Huang, F. Guo, K. Yao, Z. Lu, Y. Ma, Y. Wen, X. Dai, M. Li and X. Long, Anisotropic hydrogen bond structures and orientation dependence of shock sensitivity in crystalline 1,3,5-tri-amino-2,4,6-tri-nitrobenzene (TATB), *Phys. Chem. Chem. Phys.*, 2020, **22**, 11956.
- 23 X. Xue, Y. Wen, C. Long, J. Li and C. Zhang, Influence of Dislocations on the Shock Sensitivity of RDX: Molecular Dynamics Simulations by Reactive Force Field, *J. Phys. Chem. C*, 2015, **119**, 13735.
- 24 X. Xue, Y. Wen and C. Zhang, Early Decay Mechanism of Shocked  $\epsilon$ -CL-20: A Molecular Dynamics Simulation Study, *J. Phys. Chem. C*, 2016, **120**(38), 21169.
- 25 H. Liu, Y. Li, Z. Ma, Z. Zhou, J. Li and Y. He, Study on the Initial Decomposition Mechanism of Energetic Co-Crystal 2,4,6,8,10,12-Hexanitro-2,4,6,8,10,12-Hexaazaiso-Wurtzitane(CL-20)/1,3,5,7-Tetranitro-1,3,5,7-Tetrazacyclooctane(HMX) under a Steady Shock Wave, *Acta Phys.-Chim. Sin.*, 2019, **35**, 858.
- 26 X. Zhang, X. Chen, S. Kaliamurthi, G. Selvaraj, G. Ji and D. Wei, Initial Decomposition of the Co-crystal of CL-20/TNT: Sensitivity Decrease under Shock Loading, *J. Phys. Chem. C*, 2018, **122**, 2427.
- 27 C. Subodh, N. Ken-ichi, K. Rajiv, N. Aiichiro and V. Priya, Multiple Reaction Pathways in Shocked 2,4,6-Triamino-1,3,5-trinitrobenzene Crystal, *J. Phys. Chem. C*, 2017, **121**, 16029.
- 28 Q. An, A. William, V. Sergey, J. Andres and T. Zhou, Highly Shocked Polymer Bonded Explosives at a Nonplanar Interface: Hot-Spot Formation Leading to Detonation, *J. Phys. Chem. C*, 2013, **117**, 26551.
- 29 A. Mitchell, J. Mathew, M. Edward and S. Alejandro, Ultrafast Chemistry under Nonequilibrium Conditions and the Shock to Deflagration Transition at the Nanoscale, *J. Phys. Chem. C*, 2015, **119**, 22008.
- 30 T. Zhou, J. Lou, Y. Zhang, H. Song and F. Huang, Hot spot formation and chemical reaction initiation in shocked HMX crystals with nanovoids: a large-scale reactive molecular dynamics study, *Phys. Chem. Chem. Phys.*, 2016, **18**, 17627.
- 31 K. Yang, L. Chen, D. Liu, J. Lu, Y. Xiao, D. Geng and J. Wu, *J. Phys. Chem. C*, 2020, **124**, 10367.
- 32 <https://www.lammmps.org/>, accessed July 30, 2021.